ARTICLE

doi:10.1038/nature15750

# Measuring entanglement entropy in a quantum many-body system

Rajibul Islam[1], Ruichao Ma[1], Philipp M. Preiss[1], M. Eric Tai[1], Alexander Lukin[1], Matthew Rispoli[1] & Markus Greiner[1]

**Entanglement is one of the most intriguing features of quantum mechanics. It describes non-local correlations between quantum objects, and is at the heart of quantum information sciences. Entanglement is now being studied in diverse fields ranging from condensed matter to quantum gravity. However, measuring entanglement remains a challenge. This is especially so in systems of interacting delocalized particles, for which a direct experimental measurement of spatial entanglement has been elusive. Here, we measure entanglement in such a system of itinerant particles using quantum interference of many-body twins. Making use of our single-site-resolved control of ultracold bosonic atoms in optical lattices, we prepare two identical copies of a many-body state and interfere them. This enables us to directly measure quantum purity, Rényi entanglement entropy, and mutual information. These experiments pave the way for using entanglement to characterize quantum phases and dynamics of strongly correlated many-body systems.**

Entangled quantum objects[1] are correlated in ways that reject the principle of local realism. In few-level quantum systems, entangled states have been investigated extensively as a means of studying the foundations of quantum mechanics[2] and as a resource for quantum information applications[3]. Recently, it was realized that the concept of entanglement has broad impact in many areas of quantum many-body physics, ranging from condensed matter[4] to high-energy field theory[5] and quantum gravity[6]. In this general context, entanglement is most often quantified by the entropy of entanglement[1] that arises in a subsystem when the information about the remaining system is ignored. This entanglement entropy exhibits qualitatively different behaviour from that of classical entropy and has been used in theoretical physics to probe various properties of many-body systems. In condensed matter physics, for example, the scaling behaviour[7] of entanglement entropy allows phases to be distinguished that cannot be characterized by symmetry properties, such as topological states of matter[8–10] and spin liquids[11,12]. Entanglement entropy can be used to probe quantum criticality[13] and non-equilibrium dynamics[14,15], and to determine whether efficient numerical techniques for computing many-body physics exist[16].

Despite the growing importance of entanglement in theoretical physics, current condensed matter experiments do not have a direct probe with which to detect and measure entanglement. Synthetic quantum systems such as cold atoms[17,18], photonic networks[19], and some microscopic solid state devices[20] have unique advantages: in such systems control and detection of single particles are possible, they provide experimental access to relevant dynamical timescales, and they are isolated from the environment. In these systems, specific entangled states of few qubits, such as the highly entangled Greenberger–Horne–Zeilinger (GHZ) state[21] have been experimentally created and detected using witness operators[22]. However, entanglement witnesses are state specific. For arbitrary states, an exhaustive method of reconstructing the entire quantum state by tomography[23] can be used to measure entanglement. This has been accomplished in small systems of photonic qubits[24] and trapped ion spins[25], but there is no known way to perform tomography for systems involving itinerant delocalized particles. With multiple copies of a system, however, one can use quantum many-body interference to quantify entanglement even in itinerant systems[15,26,27].

In this work, we take advantage of the precise control and readout afforded by our quantum gas microscope[28] to prepare and interfere two identical copies of a four-site Bose–Hubbard system. This many-body quantum interference enables us to measure quantities that are not directly accessible in a single system (without tomography), for example, quadratic functions of the density matrix[15,26,27,29–32]. Such nonlinear functions can reveal entanglement[1]. In our system, we directly measure the quantum purity, Rényi entanglement entropy, and mutual information to probe the entanglement in site occupation numbers.

## Bipartite entanglement

To detect entanglement in our system, we use a fundamental property of entanglement between two subsystems (bipartite entanglement): ignoring information about one subsystem results in the other becoming a classical mixture of pure quantum states. This classical mixture in a density matrix $\rho$ can be quantified by measuring the quantum purity, defined as $\mathrm{Tr}(\rho^2)$. For a pure quantum state the density matrix is a projector and $\mathrm{Tr}(\rho^2)=1$, whereas for a mixed state $\mathrm{Tr}(\rho^2)<1$. In the case of a product state, the subsystems A and B of a many-body system AB described by a separable wavefunction $|\psi_{\mathrm{AB}}\rangle$ (Fig. 1) are individually pure as well, that is, $\mathrm{Tr}(\rho_{\mathrm{A}}^2)=\mathrm{Tr}(\rho_{\mathrm{B}}^2)=\mathrm{Tr}(\rho_{\mathrm{AB}}^2)=1$. Here the reduced density matrix of A is $\rho_{\mathrm{A}}=\mathrm{Tr}_{\mathrm{B}}(\rho_{\mathrm{AB}})$, where $\rho_{\mathrm{AB}}=|\psi_{\mathrm{AB}}\rangle\langle\psi_{\mathrm{AB}}|$ is the density matrix of the full system. $\mathrm{Tr}_{\mathrm{B}}$ indicates tracing over or ignoring all information about the subsystem B. For an entangled state, the subsystems become less pure compared to the full system as the correlations between A and B are ignored in the reduced density matrix, $\mathrm{Tr}(\rho_{\mathrm{A}}^2)=\mathrm{Tr}(\rho_{\mathrm{B}}^2)<\mathrm{Tr}(\rho_{\mathrm{AB}}^2)=1$. Even if the many-body state is mixed ($\mathrm{Tr}(\rho_{\mathrm{AB}}^2)<1$), it is still possible to measure entanglement between the subsystems[1]. It is sufficient[33] to prove this entanglement by showing that the subsystems are less pure than the full system, that is:

$$\begin{aligned}\mathrm{Tr}(\rho_{\mathrm{A}}^2)&<\mathrm{Tr}(\rho_{\mathrm{AB}}^2)\\ \mathrm{Tr}(\rho_{\mathrm{B}}^2)&<\mathrm{Tr}(\rho_{\mathrm{AB}}^2)\end{aligned}\qquad(1)$$

These inequalities provide a powerful tool with which to detect entanglement in the presence of experimental imperfections. Furthermore, quantitative bounds on the entanglement present in a mixed many-body state can be obtained from these state purities[34].

[1]Department of Physics, Harvard University, Cambridge, Massachusetts 02138, USA.



© 2015 Macmillan Publishers Limited. All rights reserved

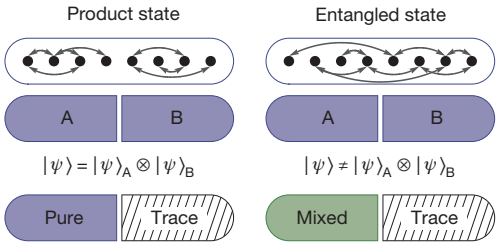


**Figure 1 | Bipartite entanglement and partial measurements.** A generic pure quantum many-body state has quantum correlations (shown as arrows) between different parts. If the system is divided into two subsystems A and B, the subsystems will be bipartite entangled with each other when there are quantum correlations between them (right column). Only when there is no bipartite entanglement present, the partitioned system $|\psi_{AB}\rangle$ can be described as a product of subsystem states $|\psi_A\rangle$ and $|\psi_B\rangle$ (left column). A path for measuring the bipartite entanglement emerges from the concept of partial measurements: ignoring all information about subsystem B (indicated as 'Trace') will put subsystem A into a statistical mixture, to a degree given by the amount of bipartite entanglement present. Finding ways of measuring the many-body quantum state purity of the system and comparing that of its subsystems would then enable measurements of entanglement. For an entangled state, the subsystems will have less purity than the full system.

Equation (1) can be framed in terms of entropic quantities[1,33]. A particularly useful and well studied quantity is the *n*th-order Rényi entropy:

$$S_n(\mathrm{A}) = \frac{1}{1-n}\log \mathrm{Tr}(\rho_\mathrm{A}^n) \tag{2}$$

From equation (2), we see that the second-order ($n=2$) Rényi entropy and purity are related by $S_2(\mathrm{A}) = -\log \mathrm{Tr}(\rho_\mathrm{A}^2)$. $S_2(\mathrm{A})$ provides a lower bound[15] for the von Neumann entanglement entropy $S_{\mathrm{VN}}(\mathrm{A}) = S_1(\mathrm{A}) = -\mathrm{Tr}(\rho_\mathrm{A}\log\rho_\mathrm{A})$, which has been extensively studied theoretically. The Rényi entropies are rapidly gaining importance in theoretical condensed matter physics because they can be used to extract information about the "entanglement spectrum"[35], thus providing more complete knowledge about the quantum state than just the von Neuman entropy. In terms of the second-order Rényi entropy, the conditions sufficient to demonstrate entanglement[1,33] become $S_2(\mathrm{A}) > S_2(\mathrm{AB})$, and $S_2(\mathrm{B}) > S_2(\mathrm{AB})$, that is, the subsystems have more entropy than the full system. These entropic inequalities are more powerful in detecting certain entangled states than other inequalities such as the Clauser–Horne–Shimony–Holt (CHSH) inequality[30,33].

## Measurement of quantum purity

The quantum purity and hence the second-order Rényi entropy can be directly measured by interfering two identical and independent copies of the quantum state on a 50%–50% beam splitter[15,26,27,30]. For two identical copies of a bosonic Fock state, the output ports always have even particle numbers, as illustrated in Fig. 2a. This is due to the destructive interference of all odd outcomes. If the system is composed of multiple modes, such as internal spin states or various lattice sites the expectation value of the total number parity $P_i = \prod_k p_i^{(k)}$ is equal to unity in the output ports $i = 1, 2$. Here the parity for mode $k$ is $p_i^{(k)} = \pm 1$ for even or odd numbers of particles, respectively.

The well known Hong–Ou–Mandel (HOM) interference of two identical single photons[36] is a special case of this scenario. Here a pair of indistinguishable photons incident upon different input ports of a 50%–50% beam splitter interfere such that both photons always exit from the same output port. In general, the average parity measured in the many-body bosonic interference on a beam splitter probes the quantum state overlap (Supplementary Information) between the two copies, $\langle P_i\rangle = \mathrm{Tr}(\rho_1\rho_2)$, where $\rho_1$ and $\rho_2$ are the density matrices of the two copies respectively and $\langle ...\rangle$ denotes averaging over repeated experimental realizations, as shown in Fig. 2b. Hence, for two identical

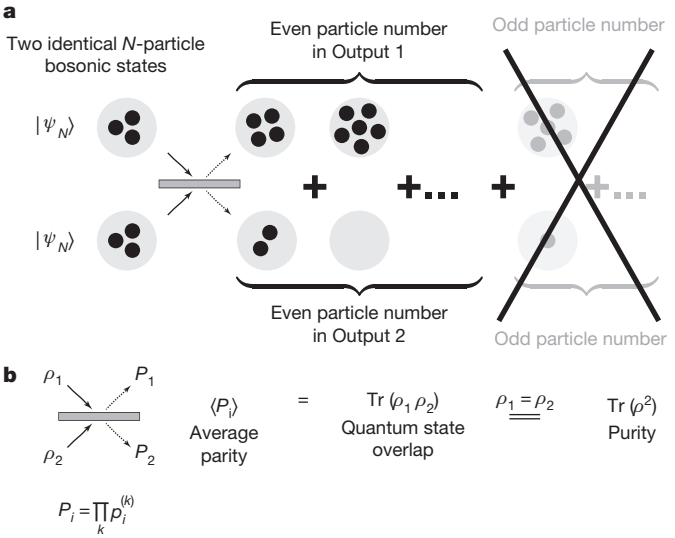


**Figure 2 | Measurement of quantum purity with many-body bosonic interference of quantum twins. a**, When two *N*-particle bosonic systems that are in identical pure quantum states are interfered on a 50%–50% beam splitter, they always produce output states with an even number of particles in each copy. This is due to the destructive interference of odd outcomes and represents a generalized HOM interference, in which two identical photons always appear in pairs after interfering on a beam splitter. **b**, If the input states $\rho_1$ and $\rho_2$ are not perfectly identical or not perfectly pure, the interference contrast is reduced. In this case the expectation value of the parity of particle number $\langle P_i\rangle$ in either output ($i = 1, 2$) measures the quantum state overlap between the two input states. For two identical input states $\rho_1 = \rho_2$, the average parity $\langle P_i\rangle$ therefore directly measures the quantum purity of the states. We assume only that the input states have no relative macroscopic phase relationship.

systems, that is, for $\rho_1 = \rho_2 = \rho$, the average parity for both output ports ($i = 1, 2$) equals the quantum purity of the many-body state[15,26,27]:

$$\langle P_i\rangle = \mathrm{Tr}(\rho^2) \tag{3}$$

Equation (3) represents the most important theoretical foundation behind this work—it connects a quantity depending on quantum coherences in the system to a simple observable in the number of particles. It holds even without fixed particle number, as long as there is no definite phase relationship between the copies (Supplementary Information). From equations (1) and (3), detecting entanglement in an experiment is thus reduced to simply measuring the average particle number parity in the output ports of the multi-mode beam splitter.

We probe entanglement formation in a system of interacting $^{87}$Rb atoms on a one-dimensional optical lattice with a lattice constant of 680 nm. The dynamics of atoms in the lattice is described by the Bose–Hubbard Hamiltonian:

$$H = -J\sum_{\langle i,j\rangle} a_i^\dagger a_j + \frac{U}{2}\sum_i n_i(n_i - 1) \tag{4}$$

where $a_i^\dagger, a_i$ and $n_i = a_i^\dagger a_i$ are the bosonic creation, annihilation, and the number operators at site $i$, respectively. The atoms tunnel between neighbouring lattice sites (indicated by $\langle i, j\rangle$) with a rate $J$ and experience an onsite repulsive interaction energy $U$. Planck's constant $h$ is set to 1 and hence both $J$ and $U$ are expressed in hertz. The dimensionless parameter $U/J$ is controlled by the depth of the optical lattice. Additionally, we can superimpose an arbitrary optical potential with the resolution of a single lattice site by using a spatial light modulator as an amplitude hologram through a high-resolution microscope (Supplementary Information). This microscope also allows us to image the number parity of each lattice site independently[28].


© 2015 Macmillan Publishers Limited. All rights reserved

To initialize two independent and identical copies of a state with fixed particle number $N$, we start with a low-entropy two-dimensional Mott insulator with unity filling in the atomic limit[28] and deterministically retain a plaquette of $2 \times N$ atoms while removing all others (Supplementary Information). This is illustrated in Fig. 3a. The plaquette of $2 \times N$ atoms contains two copies (along the $y$ direction) of an $N$-atom one-dimensional system (along the $x$ direction), with $N = 4$ in this figure. The desired quantum state is prepared by manipulating the depth of the optical lattice along $x$, varying the parameter $U/J_x$, where $J_x$ is the tunnelling rate along $x$. A box potential created by the spatial light modulator is superimposed onto this optical lattice to constrain the dynamics to the sites within each copy. During the state preparation, a deep lattice barrier separates the two copies and makes them independent of each other.

The beam splitter operation required for the many-body interference is realized in a double-well potential along $y$. The dynamics of atoms in the double well is likewise described by the Bose–Hubbard Hamiltonian, equation (4). A single atom, initially localized in one well, coherently oscillates between the wells with a Rabi frequency of $J = J_y$ (oscillation frequency in the amplitude). At discrete times during this evolution, $t = t_{\mathrm{BS}}^{(n)} = \frac{2n-1}{8J_y}$, with $n = 1, 2, \ldots$, the atom is delocalized equally over the two wells with a fixed phase relationship. Each of these times realizes a beam splitter operation, for which the same two wells serve as the input ports at time $t = 0$ and output ports at time $t = t_{\mathrm{BS}}^{(n)}$. Two indistinguishable atoms with negligible interaction strength ($U/J_y \ll 1$) in this double well will interfere as they tunnel. The dynamics of two atoms in the double well is demonstrated in Fig. 3b in terms of the joint probability $\mathcal{P}(1, 1)$ of finding them in separate wells versus the normalized time $J_y t$. The joint probability $\mathcal{P}(1, 1)$ oscillates at a frequency of 772(16) Hz $= 4J_y$, with a contrast of 95(3)%. At the beam splitter times, $t = t_{\mathrm{BS}}^{(n)}$, $\mathcal{P}(1, 1) \approx 0$. The first beam splitter time, $t_{\mathrm{BS}} \equiv t_{\mathrm{BS}}^{(1)} = \frac{1}{8J_y}$ is used for all the following experiments, with $\mathcal{P}(1, 1) = 0.05(2)$. This is a signature of bosonic interference of two indistinguishable particles[37,38], akin to the photonic HOM interference[36]. This high interference contrast indicates the near-perfect suppression of classical noise and fluctuations and includes an expected 0.6% reduction due to finite interaction strength ($U/J_y \approx 0.3$). The results from this interference can be interpreted as a measurement of the quantum purity of the initial Fock state as measured from the average parity (equation (3)), $\langle P_i \rangle = 1 - 2 \times \mathcal{P}(1, 1) = 0.90(4)$, where $i = 1, 2$ are the two copies.

## Entanglement in the ground state

The Bose–Hubbard model provides an interesting system in which to investigate entanglement. In optical lattice systems, a lower bound of the spatial entanglement has been previously estimated from time-of-flight measurements[39] and entanglement dynamics in spin degrees of freedom has been investigated with partial state reconstruction[40]. Here, we directly measure entanglement in real space occupational particle number in a site-resolved way. In the strongly interacting atomic limit of $U/J_x \gg 1$, the ground state is a Mott insulator corresponding to a Fock state of one atom at each lattice site. The quantum state has no spatial entanglement with respect to any partitioning in this phase—it is in a product state of the Fock states. As the interaction strength is reduced adiabatically, atoms begin to tunnel across the lattice sites, and ultimately the Mott insulator melts into a superfluid with a fixed atom number. The delocalization of atoms creates entanglement between spatial subsystems. This entanglement originates[41,42] from correlated fluctuations in the number of particles between the subsystems due to the super-selection rule that the total particle number in the full system is fixed, as well as coherence between various configurations without any such fluctuation.

To probe the emergence of entanglement, we first prepare the ground state of equation (4) in both copies by adiabatically lowering the optical

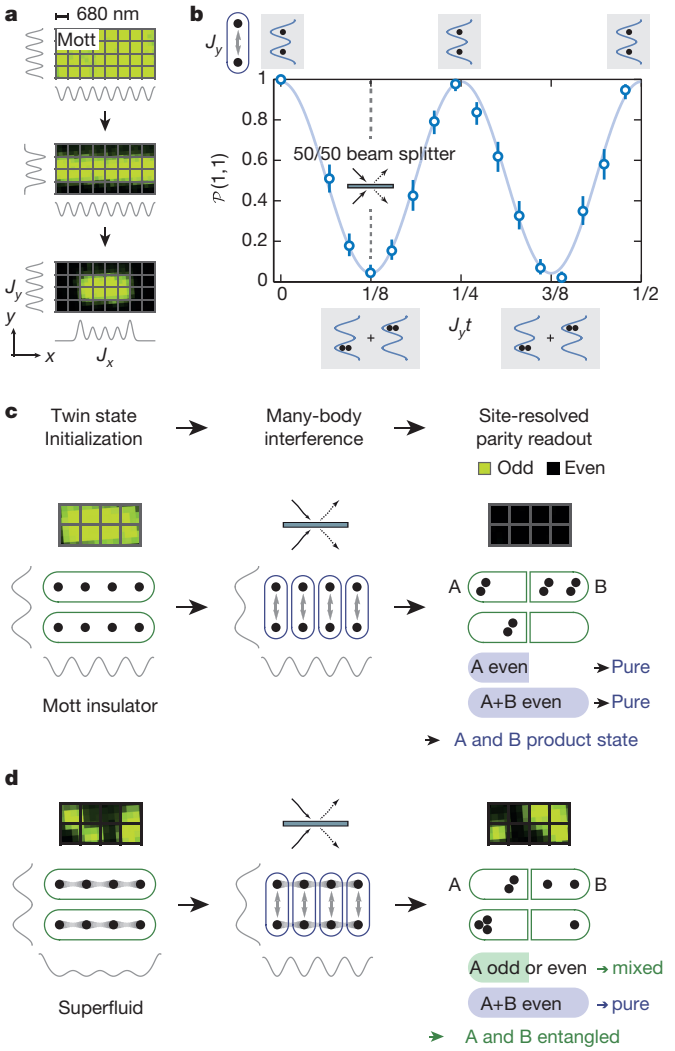


**Figure 3 | Many-body interference to probe entanglement in optical lattices. a**, A high-resolution microscope is used to directly image the number parity of ultracold bosonic atoms on each lattice site (in the raw images, green represents odd and black represents even). Two adjacent one-dimensional lattices are created by combining an optical lattice and potentials created by a spatial light modulator. We initialize two identical many-body states by filling the potentials from a low-entropy two-dimensional Mott insulator. The tunnelling rates $J_x$ and $J_y$ can be tuned independently by changing the depth of the potential. **b**, The atomic beam splitter operation is realized in a tunnel-coupled double-well potential. An atom, initially localized in one of the wells, delocalizes with equal probability into both the wells by this beam splitter. Here, we show the atomic analogue of the HOM interference of two states. The joint probability $\mathcal{P}(1, 1)$ measures the probability of coincidence detection of the atoms in separate wells as a function of normalized tunnel time $J_y t$, with the single particle tunnelling $J_y = 193(4)$ Hz. At the beam splitter duration ($J_y t = 1/8$) bosonic interference leads to a nearly vanishing $\mathcal{P}(1, 1)$, corresponding to an even parity in the output states. This can be interpreted as a measurement of the purity of the initial Fock state, here measured to be 0.90(4). The data shown here are averaged over two independent double wells. The blue curve is a maximum-likelihood fit to the data, and the error bars reflect $1\sigma$ statistical error. **c**, When two copies of a product state, such as the Mott insulator in the atomic limit, are interfered on the beam splitter, the output states contain even particle numbers globally (full system) as well as locally (subsystem), indicating pure states in both. **d**, On the other hand, for two copies of an entangled state, such as a superfluid state, the output states contain even particle numbers globally (pure state) but a mixture of odd and even outcomes locally (mixed state). This directly demonstrates entanglement.



© 2015 Macmillan Publishers Limited. All rights reserved

lattice potential along $x$. Then we freeze the tunnelling along $x$ without destroying the coherence in the many-body state and apply the beam splitter along $y$. Finally, we rapidly turn on a very deep two-dimensional lattice to suppress all tunnelling and detect the atom number parity (even = 1, odd = −1) at each site. We construct the parity of a spatial region by multiplying the parities of all the sites within that region. The average parity over repeated realizations measures the quantum purity, both globally and locally, according to equation (3), enabling us to determine the second-order Rényi entropy globally and for all possible subsystems.

In the atomic Mott insulator limit (Fig. 3c), the state is separable. Hence, the interference signal between two copies should show even parity in all subsystems, indicating a pure state with zero entanglement entropy. Towards the superfluid regime (Fig. 3d), the build-up of entanglement between various lattice sites leads to mixed states in subsystems, corresponding to a finite entanglement entropy. Hence, the measurement outcomes do not have a pre-determined parity. Remarkably, the outcomes should still retain even global parity, indicating a pure global state. Higher entropy in the subsystems than the global system cannot be explained classically and demonstrates bipartite entanglement.

Experimentally, we find exactly this behaviour for our two 4-site Bose–Hubbard systems (Fig. 4). We observe the emergence of spatial entanglement as the initial atomic Mott insulator melts into a superfluid. The measured quantum purity of the full system is about 0.6 across the Mott insulator to superfluid crossover, corresponding to a Rényi entropy of $S_2(\mathrm{AB}) \approx 0.5$. The measured purity deep in the superfluid phase is slightly reduced, probably owing to the reduced beam splitter fidelity in the presence of increased single-site occupation number, and any residual heating. The nearly constant global purity indicates a high level of coherence throughout the crossover. For lower interaction strength $U/J_x$ (superfluid regime), we observe that the subsystem Rényi entropy is higher than the full system: $S_2(\mathrm{A}) > S_2(\mathrm{AB})$. This demonstrates the presence of spatial entanglement in the superfluid state. In the Mott insulator regime ($U/J_x \gg 1$), $S_2(\mathrm{A})$ is lower than $S_2(\mathrm{AB})$ and proportional to the subsystem size, consistent with a product state.

In these measurements, we post-select outcomes of the experiment for which the total number of atoms detected in both copies is even. This constitutes about 60% of all the data, and excludes realizations with preparation errors, atom loss during the sequence, or detection errors (Supplementary Information). The measured purity is consistent with an imperfect beam splitter operation alone, suggesting much higher purity for the many-body state. The measured entropy is thus a sum of an extensive classical entropy due to the imperfections of the beam splitter and any entanglement entropy.

Our site-resolved measurement simultaneously provides information about all possible spatial partitionings of the system. Comparing the purity of all subsystems with that of the full system enables us to determine whether a quantum state has genuine spatial multipartite entanglement, in which every site is entangled with each other. Experimentally, we find that this is indeed the case for small $U/J_x$ (Fig. 4b). In the superfluid phase, all possible subsystems have more entropy than the full system, demonstrating full spatial multipartite entanglement between all four sites[27,43]. In the Mott phase ($U/J_x \gg 1$), the measured entropy is dominated by extensive classical entropy, showing a lack of entanglement.

By measuring the second-order Rényi entropy we can calculate other useful quantities, such as the associated mutual information $I_{\mathrm{AB}} = S_2(\mathrm{A}) + S_2(\mathrm{B}) - S_2(\mathrm{AB})$. Mutual information exhibits interesting scaling properties with respect to the subsystem size, which can be key to studying area laws in interacting quantum systems[44]. In some cases, such as in 'data hiding states'[45], mutual information is more informative than the more conventional two-point correlators, which might take arbitrarily small values in presence of strong correlations. Mutual information is also immune to extensive classical entropy, and hence has practical utility in the experimental study of larger systems. In our experiments (Fig. 5a), we find that for the Mott insulator state ($U/J_x \gg 1$), the entropy of the full system is the sum of the entropies for the subsystems. The mutual information is $I_{\mathrm{AB}} \approx 0$ for this state, consistent with a product state in the presence of extensive classical entropy. At $U/J_x \approx 10$, correlations between the subsystems begin to grow as the system adiabatically melts into a superfluid, resulting in non-zero mutual information, $I_{\mathrm{AB}} > 0$.

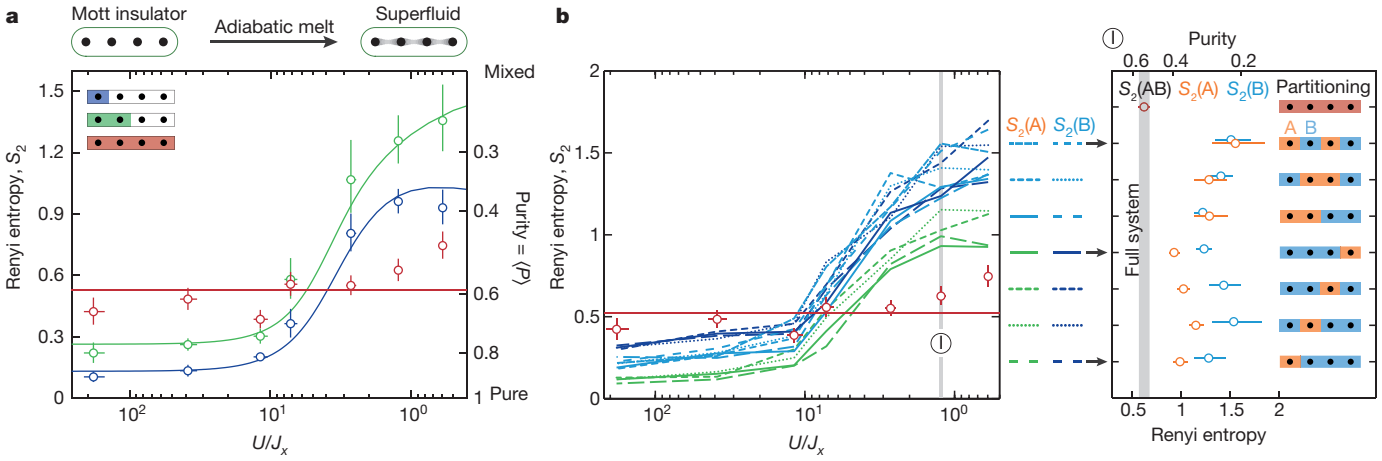


**Figure 4 | Entanglement in the ground state of the Bose–Hubbard model.** We study the transition from Mott insulator to superfluid with four atoms on four lattice sites in the ground state of the Bose–Hubbard model, equation (4). **a**. As the interaction strength $U/J_x$ is adiabatically reduced, the purity of the subsystem $A$ (green and blue, inset), $\mathrm{Tr}(\rho_A^2)$, becomes less than that of the full system (red). This demonstrates entanglement in the superfluid phase, generated by coherent tunnelling of bosons across lattice sites. In terms of the second-order Rényi entanglement entropy, $S_2(A) = -\log \mathrm{Tr}(\rho_A^2)$, the full system has less entropy than its subsystems in this state. In the Mott insulator phase ($U/J_x \gg 1$) the full system has more Rényi entropy (and less purity) than the subsystems, owing to the lack of sufficient entanglement and a contribution of classical entropy. The circles are data points and the solid lines are theoretical, calculated from exact diagonalization. The only free parameter is an added offset, assumed to be proportional to the system size and consistent with the average measured entropy (about 0.5) in the full system. The vertical error bars in this figure and in Figs 5 and 6 indicate 1$\sigma$ in combined statistical and systematic errors (Supplementary Information). **b**, Second-order Rényi entropy of all possible bi-partitioning of the system. For small $U/J_x$, all subsystems (data points connected by green and blue lines) have more entropy than the full system (red circles), indicating full multipartite entanglement[43] between the four lattice sites. The residual entropy in the Mott insulating regime is from classical entropy in the experiment, and extensive in the subsystem size. The right-hand panel in **b** shows the values of all Renyi entropies of the particular case of $U/J_x \approx 1$, to demonstrate spatial multipartite entanglement in this superfluid.



© 2015 Macmillan Publishers Limited. All rights reserved

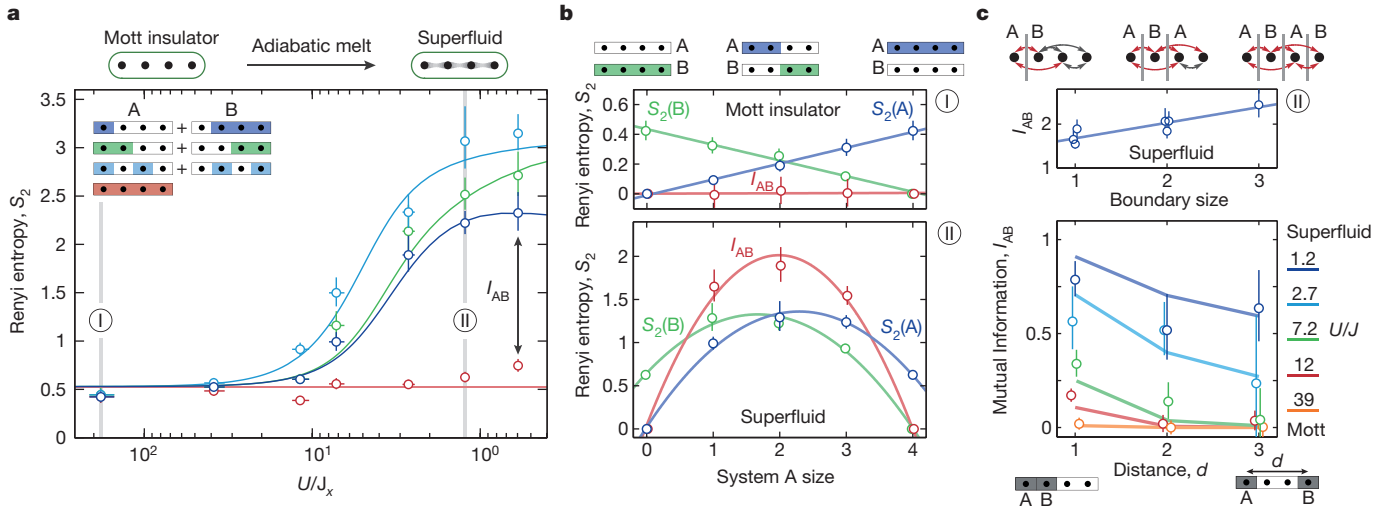


**Figure 5 | Rényi mutual information in the ground state.** Any contribution from the extensive classical entropy in our measured Rènyi entropy can be factored out by constructing the mutual information $I_{AB} = S_2(A) + S_2(B) - S_2(AB)$. **a**, We plot the summed entropy $S_2(A) + S_2(B)$ (in blue, green and light blue corresponding to the partitions shown) and the entropy of the full system $S_2(AB)$ (in red) separately. Mutual information is the difference between the two, as shown by the arrow for a partitioning scheme. In the Mott insulator phase ($U/J_x \gg 1$) the sites are not correlated, and $I_{AB} \approx 0$. Correlations start to build up for smaller $U/J_x$, resulting in a non-zero mutual information. The theory curves are from exact diagonalization, with added offsets consistent with the extensive entropy in the Mott insulator phase (about 0.5 for the full system). **b**, Classical and entanglement entropies follow qualitatively different scaling laws in a many-body system. The top panel in **b** shows that in the Mott insulator phase classical entropy dominates and $S_2(A)$ and $S_2(B)$ follow a volume law: entropy increases with the size of the subsystem. The mutual information $I_{AB} \approx 0$. The bottom panel in **b** shows the non-monotonic behaviour of $S_2(A)$ and $S_2(B)$ in the superfluid regime, due to the dominance of entanglement over classical entropy, which makes the curves asymmetric. $I_{AB}$ restores the symmetry by removing the classical uncorrelated noise. The solid lines are linear (top) and quadratic (bottom) fits included as a guide to the eye. The top panel in **c** shows that more correlations are affected (red arrow) with increasing boundary area, leading to a growth of mutual information between subsystems. The data points are for various partitioning schemes shown in Fig. 4b. The bottom panel in **c** plots $I_{AB}$ as a function of the distance $d$ between the subsystems to show the onset and spread of correlations in space, as the Mott insulator adiabatically melts into a superfluid. In these plots some overlapping data points are offset from each other horizontally for clarity.

It is instructive to investigate the scaling of Rényi entropy and mutual information with subsystem size[7,44], since in larger systems they can characterize quantum phases, for example by measuring the central charge of the underlying quantum field theory[5]. Figure 5b shows these quantities versus the subsystem size for various partitioning schemes with a single boundary. For the atomic Mott insulator the Rényi entropy increases linearly with the subsystem size and the mutual information is zero, consistent with both a product state and classical entropy being uncorrelated between various sites. In the superfluid state the measured Rényi entropy curves are asymmetric and first increase with the system size, then fall again as the subsystem size approaches that of the full system. This represents the combination of entanglement entropy and the linear classical entropy. The non-monotonicity is a signature of the entanglement entropy, as the entropy for a pure state must vanish when the subsystem size is zero or the full system. The asymmetry due to classical entropy is absent in the mutual information.

The mutual information between two subsystems comes from the correlations across their separating boundary. For a 4-site system, the boundary size ranges from one to three for various partitioning schemes. Among those schemes with a single boundary, maximum mutual information in the superfluid is obtained when the boundary divides the system symmetrically (Fig. 5a). Increasing the boundary size increases the mutual information, as more correlations are interrupted by the partitioning (Fig. 5c).

Mutual information also elucidates the onset of correlations between various sites as the few-body system crosses over from a Mott insulator to a superfluid phase. In the Mott insulator phase ($U/J_x \gg 1$) the mutual information between all sites vanish (Fig. 5c, bottom). As the particles start to tunnel, only the nearest-neighbour correlations start to build up ($U/J_x \approx 12$) and the long-range correlations remain negligible. Further into the superfluid phase, the correlations extend beyond the nearest neighbour and become long range for smaller $U/J_x$. These results suggest disparate spatial behaviour of the mutual information in the ground state of an uncorrelated (Mott insulator) and a strongly correlated phase (superfluid). For larger systems this can be exploited to identify quantum phases and the onset of quantum phase transitions.

## Non-equilibrium entanglement dynamics

Away from the ground state, the non-equilibrium dynamics of a quantum many-body system is often theoretically intractable. This is due to the growth of entanglement beyond the access of numerical techniques, such as the time-dependent density matrix renormalization group theory[46,47]. Experimental investigation of entanglement may shed valuable light onto non-equilibrium quantum dynamics. Towards this goal, we study a simple system: two particles oscillating in a double well[37,48]. The non-equilibrium dynamics are described by the Bose–Hubbard model. The quantum state of the system oscillates between unentangled (particles localized in separate wells) states and entangled states in the Hilbert space spanned by $|1, 1\rangle$, $|2, 0\rangle$ and $|0, 2\rangle$. Here, $|m, n\rangle$ denotes a state with $m$ and $n$ atoms in the two subsystems (wells), respectively. Starting from the product state $|1, 1\rangle$ the system evolves through the maximally entangled states $|2, 0\rangle + |0, 2\rangle \pm |1, 1\rangle$ and the symmetric, HOM-like state $|2, 0\rangle + |0, 2\rangle$. In the maximally entangled states the subsystems are completely mixed, with a probability of 1/3 of having zero, one or two particles. The system then returns to the initial product state $|1, 1\rangle$ before re-entangling. In our experiment, we start with a Mott insulating state ($U/J_x \gg 1$), and suddenly quench the interaction parameter to a low value, $U/J_x \approx 0.3$. The non-equilibrium dynamics is demonstrated (Fig. 6) by the oscillation in the second-order Rényi entropy of the subsystem, while the full system assumes a constant value originating from classical entropy. This experiment also demonstrates entanglement in HOM-like interference of two massive particles.

## Summary and outlook

In this work, we perform a direct measurement of quantum purity, the second-order Rényi entanglement entropy, and mutual information



© 2015 Macmillan Publishers Limited. All rights reserved

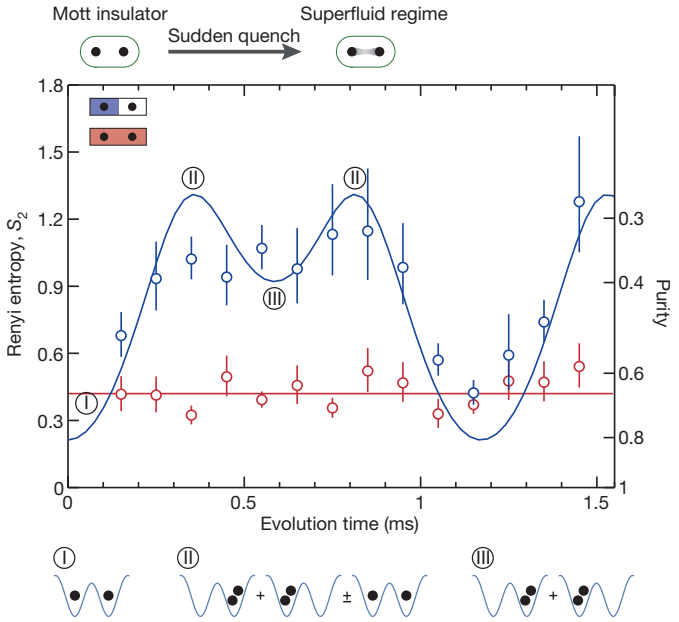


**Figure 6 | Entanglement dynamics in a quench.** Entanglement dynamics of two atoms in two sites after a sudden quench of the Hamiltonian from a large value of $U/J_x$ to $U/J_x \approx 0.3$, with $J_x \approx 210$ Hz. Here, 'evolution time' refers to the duration that the atoms spend in the shallow double well, after the initial sudden quench. The system oscillates between Mott insulator (I) and quenched superfluid regimes (II, III). The growth of bipartite entanglement in the superfluid regime is seen by comparing the measured Rényi entropy of the single site subsystem (blue data points) to that of the two site full system (red data points). The solid lines are the theoretical curves, with vertical offsets to include the classical entropy introduced by experimental imperfections.

in a Bose–Hubbard system. Our measurement scheme does not rely on full density matrix reconstruction or the use of specialized witness operators to detect entanglement. Instead, by preparing and interfering two identical copies of a many-body quantum state, we probe entanglement with the measurement of only a single operator. Our experiments represent an important demonstration of the usefulness of the many-body interference for the measurement of entanglement. It is straightforward to extend the scheme to fermionic systems[49] and systems with internal degrees of freedom[27], and to two dimensions. By generalizing the interference to $n$ copies of the quantum state[29], arbitrary observables written as an $n$th-order polynomial function of the density matrix—for example, Rényi entropies of order $n > 2$—can be measured.

With modest technical upgrades to suppress classical fluctuations and residual interactions, it should be possible to further improve the beam splitter fidelity, enabling us to work with much larger systems. Mutual information may be ideal for exploring larger systems as it is insensitive to any residual extensive classical entropy. For high entropy of a subsystem, corresponding to low state purity, the number of measurements required to reach a desired precision is high. However, in contrast to tomographic methods, this scheme would not require additional operations for larger systems. Moreover, the single-site resolution of the microscope allows us to simultaneously obtain information about all possible subsystems, to probe multipartite entanglement.

For non-equilibrium systems, entanglement entropy can grow in time (indefinitely in infinite systems). This leads to interesting many-body physics, such as thermalization in closed quantum systems[50]. The long duration of growth of entanglement entropy is considered to be a key signature of many-body localized states[14] arising in the presence of disorder. The ability to measure the quantum purity for these systems would allow experimental distinction of quantum fluctuations and classical statistical fluctuations.

More generally, by starting with two different quantum states in the two copies this scheme can be applied to measure the quantum state overlap between them. This would provide valuable information about the underlying quantum state. For example, the many-body ground state is very sensitive to perturbations near a quantum critical point. Hence, the overlap between two ground states with slightly different parameters (such as $U/J$ in the Bose–Hubbard Hamiltonian) could be used as a sensitive probe of quantum criticality[51]. Similarly the overlap of two copies undergoing non-equilibrium evolution under different perturbations can be used to probe temporal correlation functions in non-equilibrium quantum dynamics.

**Received 30 July; accepted 16 September 2015.**


1. Horodecki, R., Horodecki, P., Horodecki, M. & Horodecki, K. Quantum entanglement. *Rev. Mod. Phys.* **81,** 865 (2009).
2. Aspect, A. Bell's inequality test: more ideal than ever. *Nature* **398,** 189–190 (1999).
3. Nielsen, M. A. & Chuang, I. L. *Quantum Computation and Quantum Information* (Cambridge Univ. Press, 2010).
4. Amico, L., Fazio, R., Osterloh, A. & Vedral, V. Entanglement in many-body systems. *Rev. Mod. Phys.* **80,** 517 (2008).
5. Calabrese, P. & Cardy, J. Entanglement entropy and conformal field theory. *J. Phys. A* **42,** 504005 (2009).
6. Nishioka, T., Ryu, S. & Takayanagi, T. Holographic entanglement entropy: an overview. *J. Phys. A* **42,** 504008 (2009).
7. Eisert, J., Cramer, M. & Plenio, M. B. Colloquium: area laws for the entanglement entropy. *Rev. Mod. Phys.* **82,** 277 (2010).
8. Kitaev, A. & Preskill, J. Topological entanglement entropy. *Phys. Rev. Lett.* **96,** 110404 (2006).
9. Levin, M. & Wen, X.-G. Detecting topological order in a ground state wave function. *Phys. Rev. Lett.* **96,** 110405 (2006).
10. Jiang, H.-C., Wang, Z. & Balents, L. Identifying topological order by entanglement entropy. *Nature Phys.* **8,** 902–905 (2012).
11. Zhang, Y., Grover, T. & Vishwanath, A. Entanglement entropy of critical spin liquids. *Phys. Rev. Lett.* **107,** 067202 (2011).
12. Isakov, S. V., Hastings, M. B. & Melko, R. G. Topological entanglement entropy of a Bose–Hubbard spin liquid. *Nature Phys.* **7,** 772–775 (2011).
13. Vidal, G., Latorre, J. I., Rico, E. & Kitaev, A. Entanglement in quantum critical phenomena. *Phys. Rev. Lett.* **90,** 227902 (2003).
14. Bardarson, J. H., Pollmann, F. & Moore, J. E. Unbounded growth of entanglement in models of many-body localization. *Phys. Rev. Lett.* **109,** 017202 (2012).
15. Daley, A. J., Pichler, H., Schachenmayer, J. & Zoller, P. Measuring entanglement growth in quench dynamics of bosons in an optical lattice. *Phys. Rev. Lett.* **109,** 020505 (2012).
16. Schuch, N., Wolf, M. M., Verstraete, F. & Cirac, J. I. Entropy scaling and simulability by matrix product states. *Phys. Rev. Lett.* **100,** 030504 (2008).
17. Bloch, I., Dalibard, J. & Nascimbène, S. Quantum simulations with ultracold quantum gases. *Nature Phys.* **8,** 267–276 (2012).
18. Blatt, R. & Roos, C. F. Quantum simulations with trapped ions. *Nature Phys.* **8,** 277–284 (2012).
19. Aspuru-Guzik, A. & Walther, P. Photonic quantum simulators. *Nature Phys.* **8,** 285–291 (2012).
20. Houck, A. A., Türeci, H. E. & Koch, J. On-chip quantum simulation with superconducting circuits. *Nature Phys.* **8,** 292–299 (2012).
21. Bouwmeester, D., Pan, J.-W., Daniell, M., Weinfurter, H. & Zeilinger, A. Observation of three-photon Greenberger-Horne-Zeilinger entanglement. *Phys. Rev. Lett.* **82,** 1345–1349 (1999).
22. Gühne, O. & Tóth, G. Entanglement detection. *Phys. Rep.* **474,** 1–75 (2009).
23. James, D. F. V., Kwiat, P. G., Munro, W. J. & White, A. G. Measurement of qubits. *Phys. Rev. A* **64,** 052312 (2001).
24. Pan, J.-W. *et al.* Multiphoton entanglement and interferometry. *Rev. Mod. Phys.* **84,** 777 (2012).
25. Häffner, H. *et al.* Scalable multiparticle entanglement of trapped ions. *Nature* **438,** 643–646 (2005).
26. Ekert, A. K. *et al.* Direct estimations of linear and nonlinear functionals of a quantum state. *Phys. Rev. Lett.* **88,** 217901 (2002).
27. Moura Alves, C. & Jaksch, D. Multipartite entanglement detection in bosons. *Phys. Rev. Lett.* **93,** 110501 (2004).
28. Bakr, W. S. *et al.* Probing the superfluid–to–Mott insulator transition at the single-atom level. *Science* **329,** 547–550 (2010).
29. Brun, T. A. Measuring polynomial functions of states. *Quantum Inform. Comput.* **4,** 401–408 (2004).
30. Bovino, F. A. *et al.* Direct measurement of nonlinear properties of bipartite quantum states. *Phys. Rev. Lett.* **95,** 240407 (2005).
31. Walborn, S. P., Ribeiro, P. S., Davidovich, L., Mintert, F. & Buchleitner, A. Experimental determination of entanglement with a single measurement. *Nature* **440,** 1022–1024 (2006).
32. Schmid, C. *et al.* Experimental direct observation of mixed state entanglement. *Phys. Rev. Lett.* **101,** 260505 (2008).




© 2015 Macmillan Publishers Limited. All rights reserved

33. Horodecki, R. & Horodecki, M. Information-theoretic aspects of inseparability of mixed states. *Phys. Rev. A* **54,** 1838 (1996).
34. Mintert, F. & Buchleitner, A. Observable entanglement measure for mixed quantum states. *Phys. Rev. Lett.* **98,** 140505 (2007).
35. Li, H. & Haldane, F. D. M. Entanglement spectrum as a generalization of entanglement entropy: identification of topological order in non-abelian fractional quantum Hall effect states. *Phys. Rev. Lett.* **101,** 010504 (2008).
36. Hong, C. K., Ou, Z. Y. & Mandel, L. Measurement of subpicosecond time intervals between two photons by interference. *Phys. Rev. Lett.* **59,** 2044 (1987).
37. Kaufman, A. M. *et al.* Two-particle quantum interference in tunnel-coupled optical tweezers. *Science* **345,** 306–309 (2014).
38. Lopes, R. *et al.* Atomic Hong–Ou–Mandel experiment. *Nature* **520,** 66–68 (2015).
39. Cramer, M. *et al.* Spatial entanglement of bosons in optical lattices. *Nat. Commun.* **4,** 2161 (2013).
40. Fukuhara, T. *et al.* Spatially resolved detection of a spin-entanglement wave in a Bose–Hubbard chain. *Phys. Rev. Lett.* **115,** 035302 (2015).
41. Bartlett, S. D. & Wiseman, H. M. Entanglement constrained by superselection rules. *Phys. Rev. Lett.* **91,** 097903 (2003).
42. Schuch, N., Verstraete, F. & Cirac, J. I. Nonlocal resources in the presence of superselection rules. *Phys. Rev. Lett.* **92,** 087904 (2004).
43. Palmer, R. N., Moura Alves, C. & Jaksch, D. Detection and characterization of multipartite entanglement in optical lattices. *Phys. Rev. A* **72,** 042335 (2005).
44. Wolf, M. M., Verstraete, F., Hastings, M. B. & Cirac, J. I. Area laws in quantum systems: mutual information and correlations. *Phys. Rev. Lett.* **100,** 070502 (2008).
45. Terhal, B. M., DiVincenzo, D. P. & Leung, D. W. Hiding bits in Bell states. *Phys. Rev. Lett.* **86,** 5807–5810 (2001).
46. Vidal, G. Efficient simulation of one-dimensional quantum many-body systems. *Phys. Rev. Lett.* **93,** 040502 (2004).
47. Trotzky, S. *et al.* Probing the relaxation towards equilibrium in an isolated strongly correlated one-dimensional Bose gas. *Nature Phys.* **8,** 325–330 (2012).
48. Trotzky, S., Chen, Y.-A., Schnorrberger, U., Cheinet, P. & Bloch, I. Controlling and detecting spin correlations of ultracold atoms in optical lattices. *Phys. Rev. Lett.* **105,** 265303 (2010).
49. Pichler, H., Bonnes, L., Daley, A. J., Läuchli, A. M. & Zoller, P. Thermal versus entanglement entropy: a measurement protocol for fermionic atoms with a quantum gas microscope. *New J. Phys.* **15,** 063003 (2013).
50. Rigol, M., Dunjko, V. & Olshanii, M. Thermalization and its mechanism | for generic isolated quantum systems. *Nature* **452,** 854–858 (2008).
51. Zanardi, P. & Paunković, N. Ground state overlap and quantum phase transitions. *Phys. Rev. E* **74,** 031123 (2006).


**Supplementary Information** is available in the online version of the paper.

**Acknowledgements** We thank D. Abanin, J. I. Cirac, M. Cramer, A. Daley, A. DelMaestro, E. Demler, M. Endres, S. Gopalakrishnan, M. Headrick, A. Kaufman, M. Knap, T. Monz, A. Pal, H. Pichler, S. Sachdev, B. Swingle, P. Zoller, and M. Zwierlein for useful discussions. This work was supported by grants from the Gordon and Betty Moore Foundations EPiQS Initiative (grant GBMF3795), the NSF through the Center for Ultracold Atoms, the Army Research Office with funding from the DARPA OLE programme and a MURI programme, an Air Force Office of Scientific Research MURI programme, and an NSF Graduate Research Fellowship (to M.R.).

**Author Contributions** All authors contributed to the construction and execution of the experiments, data analysis and the writing of the manuscript.

**Author Information** Reprints and permissions information is available at www.nature.com/reprints. The authors declare no competing financial interests. Readers are welcome to comment on the online version of the paper. Correspondence and requests for materials should be addressed to M.G. (greiner@physics.harvard.edu).



© 2015 Macmillan Publishers Limited. All rights reserved